

$Z' \rightarrow e^+e^-$ studies in full simulation (DC1)

M. SCHÄFER, F. LEDROIT, B. TROCMÉ
Laboratoire de Physique Subatomique et de Cosmologie,
Grenoble, France

June 2005

Abstract

A large variety of theories beyond the Standard Model predict additional gauge bosons, or new states of the already known gauge bosons. We have selected several models featuring at least one Z' boson light enough to be detected at LHC: three configurations resulting from the breaking of the E_6 group into an effective $SU(2)_L \times U(1)_Y \times U(1)'_Y$, a left-right symmetric model and an extra dimension model with one small extra dimension. In this note, we assume that a Z' is discovered with ATLAS in the $Z' \rightarrow e^+e^-$ channel and that we now want to know which underlying theory it reveals. Two main observables are considered to discriminate between the models: the decay width times the leptonic cross section and the forward-backward asymmetry. The studies performed on fully simulated events samples are promising and are a first step toward a global discrimination procedure.



1 Introduction

Grand Unified Theories (GUTs) postulate that the $SU(3)$, $SU(2)$ and $U(1)$ symmetry groups of the Standard Model have a common origin as subgroups of some larger symmetry group G . At sufficiently large energy scale, this symmetry is supposed to be unbroken, all interactions are described by the corresponding local gauge theory and all running couplings coincide. Below some critical energy scale, G is spontaneously broken and the 3 couplings become independent. The Lie groups $SU(5)$, $SO(10)$ and E_6 are among those suggested as candidate GUT symmetries. GUT models always predict additional gauge bosons after the symmetry is broken down to the Standard Model $SU(2)_L \times U(1)_Y$ group, since W , Z , γ and g are not enough to secure local gauge invariance within a larger group. In many GUT models, the extra gauge bosons might be light enough to be accessible to colliders.

Other examples of extensions of the SM are string theory or extra dimensions. In string theory, the fundamental objects are one-dimensional strings rather than points in space. A string can have excitations and the zero mass modes can represent fundamental particle states. Extra dimensions are either compactified, so that we could not yet have accessed them, or they are seen only by gravitation. In either case, extra gauge bosons are predicted.

A non exhaustive list of models predicting new vector bosons includes: effective rank-5 models ($E6$) [1]-[6], left-right symmetric models (LR or LRM) [7, 6], alternative left-right symmetric models ($ALRM$) [7, 6], the Sequential Standard Model (SSM) [6], the Un-unified Standard Model ($UNSM$) [8, 6], the Foot-Hernandez model [9], the model of Kuo [10], the BESS model [11], the little Higgs model [12], warped Higgsless models [13], several extra dimension scenarios [14],... A narrow graviton resonance (tensor boson) [15] in the Randall-Sundrum model is another popular candidate of extra dimension models.

The search for these particles is an important aspect of the experimental high-energy physics program. The LHC discovery potential for a Z' as a mass peak above a small background in the reaction $pp \rightarrow Z' \rightarrow l^+l^-$ is high and well known [16]. The luminosity required to discover the Z' in this channel depends only on the cross section times leptonic branching ratio, and therefore on its mass and couplings. Once a Z' boson is observed at the LHC, one will want to discriminate between the different models which can yield such a resonance. Several observables have been proposed in [16]: in addition to the total width and cross section, forward-backward asymmetry provide information about the Z' couplings and its interference with the Z boson and the photon. Furthermore, one can include the analysis of the Z' rapidity distribution, which is sensitive to the Z' couplings to u and d quarks.

In this work the process $Z' \rightarrow e^+e^-$ was studied for Z' masses of 1.5 TeV and 4 TeV. The first value was chosen as it is realistic regarding the present limits and for comparison purpose with other studies. Furthermore, it is a reasonable value for studies at $10 fb^{-1}$ which offers interesting possibilities for the commissioning period of the ATLAS detector.

The present document is organized as follows: in the next section we present the specific models used. In section 3, Z' production and decay, the expected background and the Z' discovery limits are discussed. In section 4, the event generation and simulation is presented; in section 5, the reconstruction performance is shown together with the

event selection. In section 6, we describe a first set of relevant observables that can be measured with ATLAS, namely the total decay width and the leptonic cross section and perform their measurement on fully simulated data. An additional observable, the forward-backward asymmetry, is treated separately in section 7. Finally, the prospects for discrimination between different models are discussed (section 8).

2 Specific models

- A popular model is an effective $SU(2)_L \times U(1)_Y \times U(1)'_Y$ model, originating from the breaking of the E_6 group, which is general enough to include many interesting possibilities [3]. Indeed, in the breaking of this group down to the SM symmetry, two additional neutral gauge bosons could appear. For simplicity it is assumed that only the lightest Z' can be produced at LHC. This extra boson is uniquely determined by a new mixing angle θ , that fixes the combination of two independent $U(1)$ bosons arbitrarily chosen in E_6 [4]¹:

$$Z' = \cos \theta Z'_\psi - \sin \theta Z'_\chi.$$

The general neutral current Lagrangian reads in the case of one extra $U(1)'$ [5]:

$$-\mathcal{L}_{NC} = \bar{\Psi}_k \gamma^\mu [T_{3k} g W_{3\mu} + Y_k g_{11} B_\mu + Y_k g_{12} Z'_\mu + Q'_k g_{22} Z'_\mu] \Psi_k,$$

where T_3 and Y are the standard isospin and hypercharge, Q' is the extra $U(1)'$ charge. The coefficients g_{11} , g_{12} , g_{22} are measurable couplings.

The cases $\theta = 0, -\frac{\pi}{2}, \arctan(-\sqrt{\frac{5}{3}}) + \frac{\pi}{2}$ are called Z'_ψ, Z'_χ and Z'_η ². In these cases, $g_{12} = 0$ and $g_{22} = g_{11}$. The Q' charges are given in table 1.

- Z'_ψ model: $E_6 \rightarrow SO(10) \times U(1)_\psi$
- Z'_χ model: $E_6 \rightarrow SO(10) \times U(1)_\psi \rightarrow SU(5) \times U(1)_\chi \times U(1)_\psi$
- Z'_η model: E_6 breaks directly down to a rank 5 group
 $E_6 \rightarrow SU(3)_C \times SU(2)_L \times U(1)_Y \times U(1)_\eta = SM \times U(1)_\eta$

Q'	$2\sqrt{10}Q_\chi$	$2\sqrt{6}Q_\psi$	$2\sqrt{15}Q_\eta$
u_L, d_L	-1	1	-2
u_R	-1	1	-2
d_R	3	1	1
ν_L, l_L	3	1	1
l_R	-1	1	-2

Table 1: Q' charges

- Other popular models are the left-right (LR) models [7]. They are based, for example, on the simplest extended gauge group which introduces charged current interactions for the right-handed fermions and results from the breaking down of $SO(10)$:

$$SO(10) \rightarrow SU(3)_C \times SU(2)_L \times SU(2)_R \times U(1)_{B-L},$$

¹In the literature[5, 6, 16], the coupling constants are often described as a function of a translated angle $\beta = \theta + \pi/2$.

²following the convention of Ref. [3], which corresponds to $\theta + \pi$ in Refs. [5, 16].

where B and L are the baryon and lepton numbers. They are parametrized by the ratio $\kappa = \frac{g_R}{g_L}$ of the gauge couplings from $SU(2)_{L,R}$. With the same notation as above, one can write $Q_{LR} = Q_\chi$, $g_{22} = \frac{e}{\cos\theta_w} \sqrt{\frac{2}{5} \frac{\alpha_{LR}^2 + 1}{\alpha_{LR}}}$ and $\frac{g_{12}}{g_{22}} = \sqrt{\frac{1}{6} \frac{3\alpha_{LR}^2 - 2}{\alpha_{LR}^2 + 1}}$, with $\alpha_{LR} = \sqrt{\frac{\cos^2\theta_w}{\sin^2\theta_w} \kappa^2 - 1}$. We will assume $\kappa = 1$, which corresponds to manifest left-right symmetric gauge interactions.

- For a complete comparison, we will also discuss the case of a sequential boson Z'_{SSM} , which has the same couplings to fermions as the SM Z boson.

In table 2, all coupling constants of the models above are shown. In these extended electroweak models, one must consider the possibility of mixing between the ordinary Z gauge boson and the new one(s). Such mixing can fortunately be neglected as the observed Z mass agrees very well with the predictions from the Standard Model $SU(2)_L \times U(1)_Y$ if the new gauge bosons are heavy, i.e. ≥ 1 TeV [1].

	g_V	g_A
	ψ, χ, η	
ν	$\frac{1}{6} \sqrt{\frac{5}{2}} \cos\theta - \frac{3}{2} \sqrt{\frac{1}{6}} \sin\theta$	$\frac{1}{6} \sqrt{\frac{5}{2}} \cos\theta - \frac{3}{2} \sqrt{\frac{1}{6}} \sin\theta$
e	$-\frac{2}{\sqrt{6}} \sin\theta$	$\frac{1}{3} \sqrt{\frac{5}{2}} \cos\theta - \sqrt{\frac{1}{6}} \sin\theta$
u	0	$\frac{1}{3} \sqrt{\frac{5}{2}} \cos\theta + \sqrt{\frac{1}{6}} \sin\theta$
d	$\frac{2}{\sqrt{6}} \sin\theta$	$\frac{1}{3} \sqrt{\frac{5}{2}} \cos\theta - \sqrt{\frac{1}{6}} \sin\theta$
	LR	
ν	$\frac{1}{2\alpha_{LR}}$	$\frac{1}{2\alpha_{LR}}$
e	$\frac{1}{\alpha_{LR}} - \frac{1}{2}\alpha_{LR}$	$\frac{1}{2}\alpha_{LR}$
u	$-\frac{1}{3\alpha_{LR}} + \frac{1}{2}\alpha_{LR}$	$-\frac{1}{2}\alpha_{LR}$
d	$\frac{-1}{3\alpha_{LR}} - \frac{1}{2}\alpha_{LR}$	$\frac{1}{2}\alpha_{LR}$

Table 2: *Coupling constants*

- Extra dimensions, Z'_{KK} ([17] and references therein)
 In models with “large” extra dimensions, characterized by compactification radii $\gg 1 \text{ TeV}^{-1}$, gravity propagates in the bulk, and the SM fields are confined to a 3-brane since gauge interactions are known up to this scale. The presence of the extra dimensions could be probed by searching for the Kaluza-Klein excitations of the graviton. An interesting variation of these models assumes that only the fermions are confined in the 3-brane, whereas the gauge fields propagate also in a number of additional small extra dimensions, orthogonal to the brane, with compactification radius $\sim (1 \text{ TeV})^{-1}$.
 The model used here was motivated by the ATLAS study in [18]. One “small” extra dimension compactified on S^1/Z_2 is considered. The model is completely specified by a single parameter M_C , the compactification scale. The main signature for this model is the appearance of a tower of Kaluza-Klein (KK) resonances for each of the gauge fields propagating in the bulk. The masses M_n of the KK modes are given by the relation $M_n^2 = (nM_C)^2 + M_0^2$, where M_0 is the mass of

the zero-mode excitation corresponding to the Standard Model gauge boson. The couplings for the resonances of the photon and the Z boson are the same as the corresponding SM couplings, scaled by a factor $\sqrt{2}$. Even with only one small extra dimension, the excitations of the γ , Z and W bosons are nearly degenerate in mass. The first neutral resonance which could be observed is made of the first KK mode of the photon and of the Z with their interference.

The graviton [15] could give the same signature as a Z' in models of warped extra dimensions, but this case is not considered here.

3 Searching for a Z' boson at the LHC

3.1 Production and decay

In a hadron collider, the dominant Z' production process is $q\bar{q} \rightarrow Z'$. Considering only decays into known particles, the most efficient way of observing new gauge bosons in a pp -collider is to identify charged leptons in the final state: $pp \rightarrow l^+l^-X$, since hadronic decays ($Z' \rightarrow q\bar{q}$) are difficult to detect in the QCD background. Decays such as $Z' \rightarrow W^+W^-$, $f\bar{f}Z$, $f\bar{f}W$, $Z'Z$, $Z'\gamma$ are expected to be rare [19, 20]. The Z' boson can also decay to NN , where N is a Majorana neutrino; the corresponding branching ratio depends on the mass of the neutrino. A study of this decay can be found in [21].

The unpolarized differential cross section for the process $pp \rightarrow Z' \rightarrow l^+l^-X$ depends on the effective Z' mass $\sqrt{s'}$, on the Z' rapidity Y and on the angle θ^* , defined as the angle between the negatively charged lepton and the quark in the center of mass of the colliding partons (see figure 1). The general form of this cross section is [2]:

$$\frac{d\sigma}{d\sqrt{s'}dYd\cos\theta^*} = \sum_{\text{quarks } q} [g_q^S(Y, \sqrt{s'})S_q(\sqrt{s'})(1 + \cos^2\theta^*) + g_q^A(Y, \sqrt{s'})A_q(\sqrt{s'})2\cos\theta^*], \quad (1)$$

where S_q and A_q are the only model-dependent quantities, containing the couplings of quarks and leptons to the different neutral gauge bosons while g_q^S and g_q^A involve the parton distribution functions of the colliding hadrons.

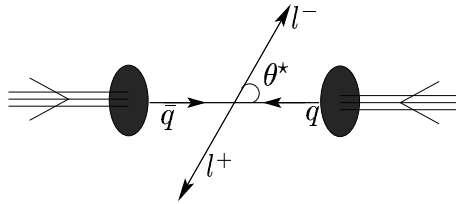


Figure 1: l^+l^- production in $p\bar{p}$ collisions, $\theta^* = \angle(e^-, q)_{Z'}$

Leptonic decay channels with ATLAS

e^+e^- . This channel is the most promising, as the detector resolution may be good enough to measure the natural width, as shown in [18]. The energy resolution of the electromagnetic calorimeter is dominated at high energy ($E > 200$ GeV) by the global constant term which is estimated at $\sim 0.7\%$, i.e. a resolution of 10 GeV for 1.5 TeV electrons, neglecting photon radiation and assuming that the resolution extrapolates

perfectly at very high energy.

$\mu^+\mu^-$. The momentum resolution in the muon spectrometer should be such that the mass of a 3 TeV Z' may be measured with a 8% precision, which is generally higher than the expected natural decay width. A study of this channel was already performed in [22].

$\tau^+\tau^-$. The kinematics of $Z' \rightarrow \tau^+\tau^-$ events [23] are sufficiently constrained to allow reconstruction of the momenta of both τ 's [24]. In the τ channel, further information can be extracted from the polarization asymmetry, the production asymmetry of left and right handed τ 's.

In the following we have chosen to concentrate on the e^+e^- channel.

3.2 Physical background

The $Z' \rightarrow e^+e^-$ channel has two advantages. First, it benefits from the high detector resolution of ATLAS for electrons and second, it is a very clean channel. As backgrounds, all the processes yielding e^+e^- pairs have to be considered, as well as all processes including an electron (or positron) and a photon, which can be misidentified as an electron. The main processes are: Drell-Yan³, ZZ , ZW^\pm , W^+W^- , $Z\gamma$, $W^\pm\gamma$, $t\bar{t}$, $b\bar{b}$. The dijets mis-tagged as electrons are not evaluated here. The $b\bar{b}$ case can be excluded by a p_T cut. In principle, the $Z' + DY \rightarrow \tau\tau$ process where both τ 's decay to an electron has to be considered as well. This produces some additional background and a deformation of the DY background shape. Nevertheless, it should be rather negligible because of the low branching ratio and because a selection criteria on the angle between the two electrons should be very efficient in removing it.

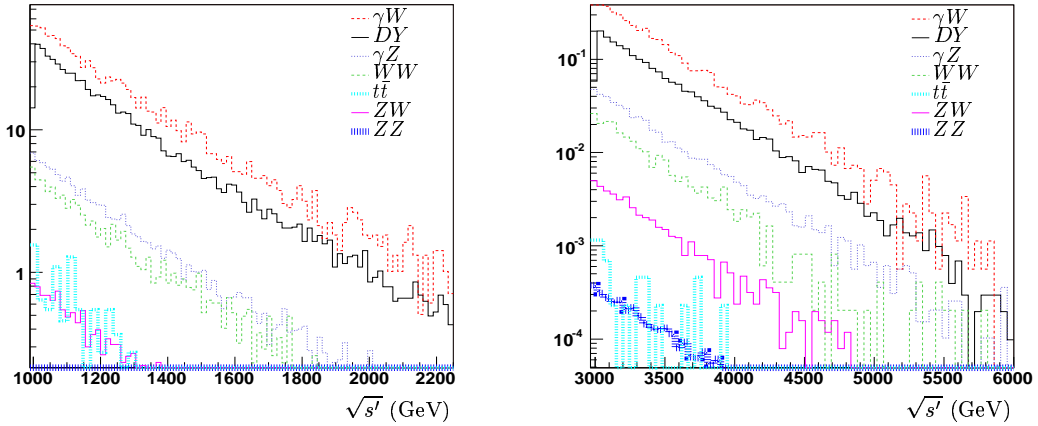


Figure 2: *Dilepton invariant mass for background processes for 100fb^{-1}*

In Fig. 2, the numbers of expected events without any selection are given for the Drell-Yan process and the different backgrounds in $\sqrt{s'}$ windows around 1.5 TeV and 4 TeV. With its large cross section, the $W\gamma$ background is the main potential contamination

³The Drell-Yan is a process which interferes with Z' production and therefore cannot, strictly speaking, be considered separately from it. However, it is presented here as a “background” in order to give an estimate of the level of the non-resonant signal.

source; it however may be easily reduced because of the high photon rejection factor (see section 5.1).

3.3 Limits from existing data and Z' reach with ATLAS

Limits on the existence of a Z' may be divided into two categories: limits from direct search, and limits from indirect measurements (fits to precision electro-weak data). Both direct and indirect searches lead to model-dependent constraints. The present Z' mass limits for the different models vary between 350 GeV and 1500 GeV with a good agreement between direct and indirect measurements [17, 25, 26]. In the case of a Z' with suppressed or no couplings to leptons (i.e. a leptophobic Z' [27]), the experimental limits are much weaker. Searches at CDF for new particles decaying to dijets [28] are indeed unable to rule out a Z' for the SSM case in any mass region. The limit in the KK case is at about 4 TeV in the hypothesis of a light SM Higgs boson propagating in higher dimensions. In the case where the Higgs boson (up to 500 GeV mass) is trapped in the 3-brane, relatively light KK mass scales are possible [29]. In Higgsless models, lighter KK gauge bosons are possible as well [30], with different couplings.

The ATLAS discovery potential for a Z' boson has been evaluated in the TDR [31]; Z' from E_6 and LR models can be discovered at 5σ confidence level for masses at least up to 5 TeV. Moreover, in other models, a careful analysis of ATLAS data could conclude on the presence of resonances up to 11 TeV for $300 fb^{-1}$ [18].

4 Event generation and simulation

4.1 Samples

Events are generated with PYTHIA 6.2 [32] within ATHENA release 7.0.2 [33]. The Z' boson is generated in the $pp \rightarrow Z' \rightarrow e^+e^-$ channel at masses of 1.5 TeV and 4 TeV. For the different E_6 models, the LR model and the SSM , the couplings g_V and g_A are varied. For the Z'_{KK} , a user defined external process was interfaced to ATHENA⁴: the full Breit-Wigner shape for the first two excitations of the photon and the Z boson are included; the higher lying states are re-summed.

The CTEQ5L parton distribution function is used and initial/final state radiations are switched on. The Z' production being very sensitive to the Drell-Yan production, both processes are produced at the same time with the complete interference structure. The detailed characteristics of the generated samples are given in table 3. At $M=1.5$ TeV, the number of events has been chosen such that the peak region contains around 10000 events. The simulation was made at CERN in the framework of DC1 (Data Challenge 1 [37] with GEANT 3 [38], ATHENA release 7.0.0), only particles with a pseudo rapidity in the range $[-2.5;2.5]$ being taken into account. Reconstruction was done within ATHENA release 7.0.2, without electronic noise and pile-up (this should however have a minor impact on the considered studies); the final detector layout was used.

⁴External process for PYTHIA: T.Rizzo and G.Azuelos [18], interface to ATHENA M.Schäfer.

		$\int \mathcal{L}(fb^{-1})$	Cross section (fb)	Minimal $\sqrt{s'}$ (GeV)
$M = 1.5 \text{ TeV}$	SSM	122	164.4	500
	ψ	321	124.9	500
	χ	131	153.1	500
	η	312	128.2	500
	LR	135	148.6	500
$M = 4 \text{ TeV}$	SSM	500	0.4	2000
	KK	517	5.9	1000

Table 3: Simulated integrated luminosities, cross section and lower cut on $\sqrt{s'}$ for the generated samples.

4.2 Kinematics of the Z' boson

In figure 3, are presented several kinematic characteristics for the SSM at generation level: the Z' rapidity, the lepton transverse momentum, their pseudorapidity, and the opening angle between them in the transverse plane, $\Delta\phi$. The relative abundance of the different flavour types in the quark/antiquark system is given for all models in table 4.

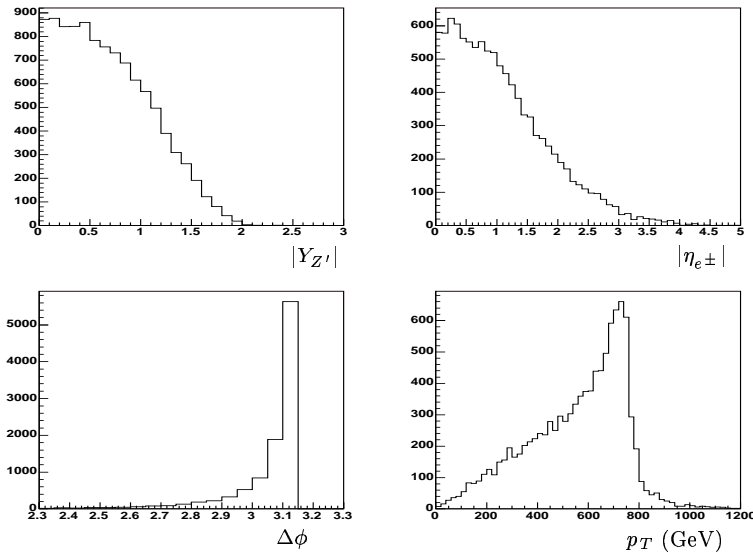


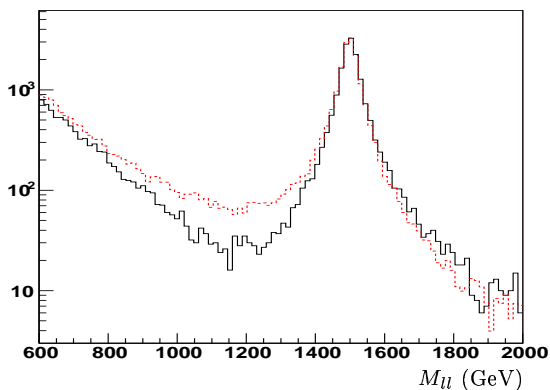
Figure 3: Kinematics for $\sqrt{s'} > 1 \text{ TeV}$ - Z'_{SSM} model - $M = 1.5 \text{ TeV}$

4.3 Z' - DY interference

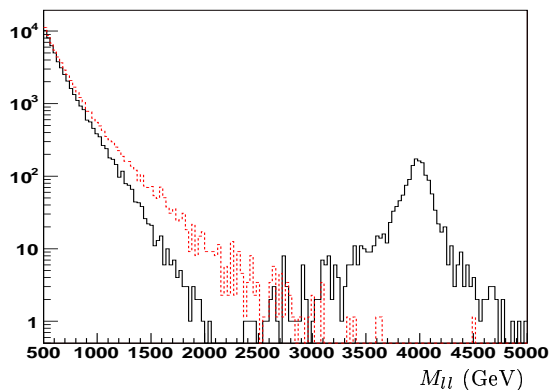
The effect of the interference in the Z'_{SSM} model at $M=1.5 \text{ TeV}$ is shown in Fig. 4(a): a distortion of the peak is observable, especially for the lower masses, where the effect is found to be largely destructive. This effect is even more striking in the KK case at $M=4 \text{ TeV}$ represented in Fig. 4(b).

		d	u	Others
$M = 1.5 \text{ TeV}$	SSM	40.9 ± 0.8	55.3 ± 0.9	3.7 ± 0.2
	χ	70.3 ± 1.4	24.3 ± 0.7	5.4 ± 0.3
	η	25.6 ± 0.6	71.7 ± 1.2	2.7 ± 0.2
	ψ	34.4 ± 0.8	62.2 ± 1.1	3.3 ± 0.2
	LR	48.2 ± 1.0	47.6 ± 1.0	4.2 ± 0.2
$M = 4 \text{ TeV}$	SSM	65.4 ± 1.2	33.7 ± 0.8	0.9 ± 0.1
	KK	85.5 ± 3.7	14.3 ± 1.2	0.2 ± 0.1

Table 4: Abundance at generation level of flavour types (in percentage) of the quark/antiquark system at $M=1.5 \text{ TeV}$ for $\sqrt{s'} > 1.4 \text{ TeV}$



(a) Z'_{SSM} model - $M = 1.5 \text{ TeV}$ (black/solid with interference, red/dashed without)



(b) Z'_{KK} model - $M = 4 \text{ TeV}$ (black/solid with interference, red/dashed DY only)

Figure 4: Interference effects

5 Event reconstruction and selection

5.1 Electron identification

Electrons coming from Z' decays are expected to be isolated. For this study, available single electrons, single photons and dijets samples from the DC1 production are used. Only clusters with a transverse energy higher than 50 GeV are taken into account. The preliminary electron-identification variable of ATHENA 'ISEM' is used [39] - even if it was optimized for low energy electrons. This variable includes criteria on the shower shape and on the energy leakage in the hadronic calorimeter. At least one isolated matched track is required, cluster candidates with more than one extra-track in a broad window (0.05 in η and 0.1 in ϕ) around the matched track are excluded. To reject photons, a good track quality is required, i.e. a high total number of hits (≥ 6) in the tracker.

With these very simple criteria, the efficiencies presented in table 5 are obtained. The low photon misidentification probability is only due to the track matching criteria and could be improved with a dedicated study.

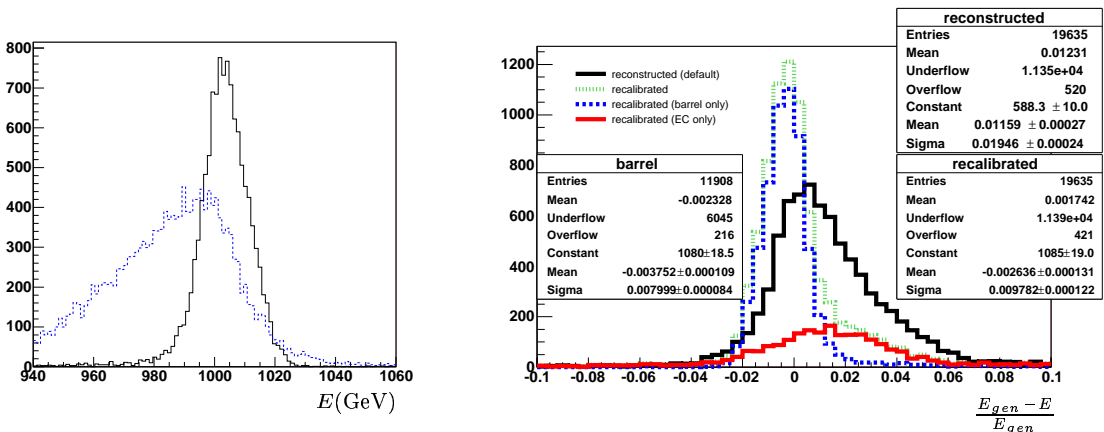
single electrons 200 GeV	91%
single electrons 1 TeV	87%
single photons 200 GeV	4 %
dijets 560 GeV	0.13%

Table 5: *Electron identification : selection rates*

5.2 Electron energy calibration in ATHENA

At present, the calibration is done at cell level (see [40] and references therein), with all weights and corrections optimized on photons. So, for electrons, one has to “de-calibrate” and to “re-calibrate” [40]. Of course this is only a stopgap until separate photon and electron calibration will be implemented in ATHENA.

This procedure is only finalized for the barrel, as the current photon weights are calculated with an incomplete end-cap simulation. It was finalized and tested on the $H \rightarrow 4e$ process, i.e. on lower energy electrons. The procedure is tested on higher energy single electrons datasets to justify that it can also be applied to more energetic electrons, as expected from Z' decays.



(a) *Energy* (blue/dashed line: standard calibration, black/solid line: electron calibration)

(b) *Resolution*

Figure 5: *Single electrons, 1 TeV from DC1*

In figure 5, the results at 1 TeV are presented. The obtained resolution is slightly worse than the expected resolution (0.8% instead of $\frac{\sigma(E)}{E} = \frac{9.5\%}{\sqrt{E}} \oplus 0.45\% = 0.5\%$). However, after the calibration, the energy measurement is found to be unbiased; this procedure will therefore be used for the Z' electrons.

5.3 Electron charge determination

The wrong assignment of the charge sign of the leptons leads to an error on the forward-backward asymmetry.

In the single electron samples from DC1 at 1 TeV, the charge sign was found to be

wrong in 5% of the events; this is in a relative agreement with the TDR prediction of 3.6%[31].

In the Z'_{SSM} sample at 1.5 TeV, in 6.5% of the events the two leptons do not have opposite charges. This corresponds to 3.4% for the probability of the wrong assignment of a single lepton, which is consistent with the results of the single electrons samples. The probability that both leptons are assigned the wrong charge is thus negligible (1 per mil). At 4 TeV, the individual wrong charge assignment probability increases to 11%, and the probability of double wrong assignment therefore reaches about 1%.

5.4 Event selection

Only events with two identified electrons are kept. Additionally, electrons are required to be isolated in the calorimeter: there must be no cluster with $E_T > 40$ GeV in a cone of radius $\sqrt{\Delta\phi^2 + \Delta\eta^2} = 0.5$. The loss in efficiency due to this criterion is negligible. Furthermore, the two electrons are required to have opposite charges and to be back to back: the angle in the transverse plane between the two leptons in the laboratory frame must be greater than 2.9 radians. This selection criterion not only allows to reject some background, but also insures that the quark direction is not heavily affected by initial state radiation. A total acceptance of about 46% on average is achieved in the full simulated mass range.

Besides, only the events with both leptons in the barrel ($|\eta| \leq 1.5$) are taken into account in the study of the decay width and the cross section. Excluding the events with one or two leptons in the end-cap, the average acceptance is reduced to about 28%. The efficiency of the above selections is presented as an example for the SSM in table 6.

initial events	20000
at least two electrons with $ \eta < 2.5$	16425
at least two identified and isolated electrons	11418
opposite charge	10683
back to back	9184
accepted (all)	9184
accepted (barrel)	5626

Table 6: *Selection efficiencies - Z'_{SSM} model - $M = 1.5$ TeV*

5.5 Resolution and acceptance

The resolution on the reconstruction of the pseudo rapidity η of the electrons and positrons is shown in Fig. 6. There is no bias.

In the dielectron invariant mass computation, the following definition of the electron 4-momentum is used:

$$\begin{aligned}
 E &= E_t^{calo} \times \sqrt{\cot^2 \theta_{track} + 1} \\
 p_x &= E_t^{calo} \times \cos \phi_{track} \\
 p_y &= E_t^{calo} \times \sin \phi_{track} \\
 p_z &= E_t^{calo} \times \cot \theta_{track}
 \end{aligned}$$

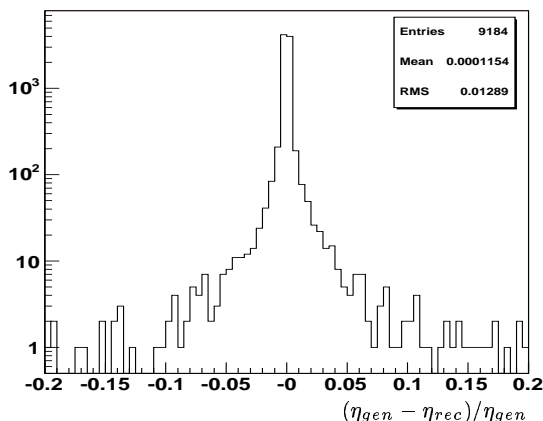


Figure 6: *Pseudo rapidity resolution - Z'_{SSM} model - $M = 1.5 \text{ TeV}$*

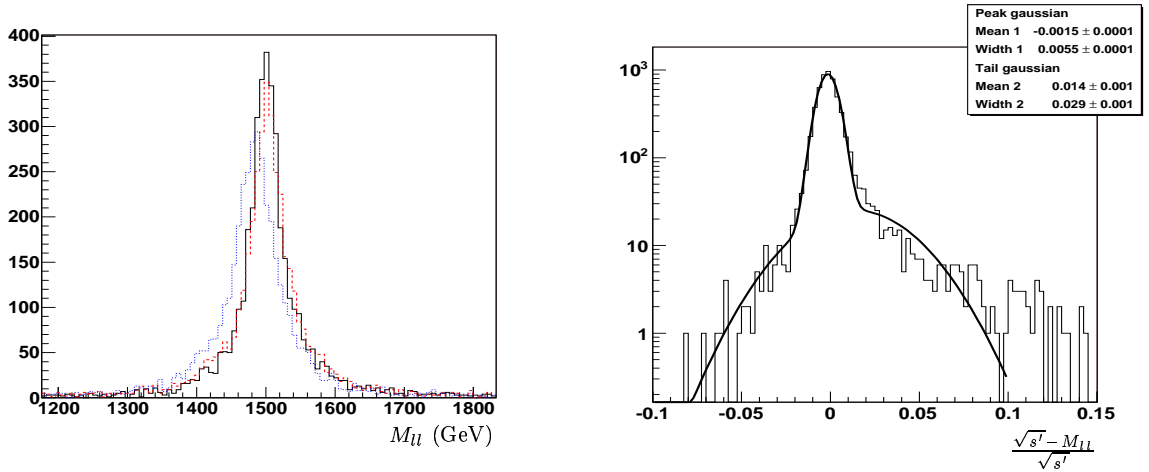
The effect of the calibration on the dielectron mass distribution is shown for the Z'_{SSM} model at 1.5 TeV in figure 7. Only barrel electrons are used. In figure 7(a) the mass distributions themselves are shown: truth, before and after re-calibration. With the standard calibration the mass is underestimated, this bias vanishing after the re-calibration. The smearing effect of the detector resolution can be seen. In figure 7(b), this resolution is quantified: for most of the events, the resolution is gaussian with a σ of about 8 GeV, i.e. $\frac{\sigma(E)}{E} = 0.75\%$, which is consistent with the resolution observed in the case of the single electrons sample. In addition, there are small tails, which are on the one hand due to Bremsstrahlung (in the positive region) and on the other hand to this temporary de- and re-calibration procedure. In all the following, this resolution is modelised by a the sum of two gaussian functions, which characteristics are given in Fig. 7(b); the peak Gaussian is found to contain 87% of the events.

The acceptance as a function of the mass is shown in Fig. 8 for the same model. It is around 49% in the resonance region (34%, when requiring the two electrons to be in the barrel); the electron reconstruction efficiency being not uniform in the detector, and the pseudo rapidity distribution of the electrons depending on the model, this mass acceptance is slightly model dependent (in the range 32.4 to 35.4% for the barrel).

6 Total decay width times leptonic cross section as a probe of the underlying model

6.1 Theoretical predictions

In the absence of any exotic decay channel, the total decay width is given by the sum of the partial decay widths to neutrinos, leptons and quarks of all 3 generations. Only fermionic decay channels are implemented in the generation program; rare decays such



(a) *Black/solid line: truth, blue/dashed: reconstructed, red/dotted: re-calibrated*

(b) *Mass resolution*

Figure 7: *Effect of the re-calibration on the mass - Z'_{SSM} model - $M = 1.5 \text{ TeV}$*

as $Z' \rightarrow W^+W^-$ are not included. The partial decay width is given by

$$\Gamma(Z' \rightarrow f\bar{f}) = N_c \frac{e^2}{\cos^2 \theta_w} \frac{1}{48\pi} (g_V^2 + g_A^2) M$$

where N_c is a color factor⁵ and where the couplings g_A, g_V are given in table 2. The resulting total decay width is shown in figure 9 as a function of the model parameter: θ for the E_6 models, and κ for the LR models. The different branching ratios $Br(i) = Br(Z' \rightarrow i\bar{i}), i = u, d, e, \nu$ are shown in the same figure. The numerical results are given in table 7 for the studied values of the parameters.

	Γ/M
SSM	0.030
ψ	0.005
χ	0.012
η	0.006
LR	0.020

Table 7: *Theoretical total decay width*

The formula used above is valid for negligible fermion masses. Correcting for the top quark mass would lead to a little smaller $\frac{\Gamma}{M}$ depending on the models [24]. The partial decay width to quarks should also undergo small corrections due to final-state QCD interactions.

The leptonic cross section is defined as $\sigma_{ll} = \sigma \times Br(Z' \rightarrow ll)$. Both the leptonic cross section and the total width are altered if exotic decays of the Z' boson are present, e.g. decay into gauginos $Z' \rightarrow \tilde{\chi}_i \tilde{\chi}_j$ [4]. However, this dependence disappears in the

⁵1 for leptons, 3 for quarks.

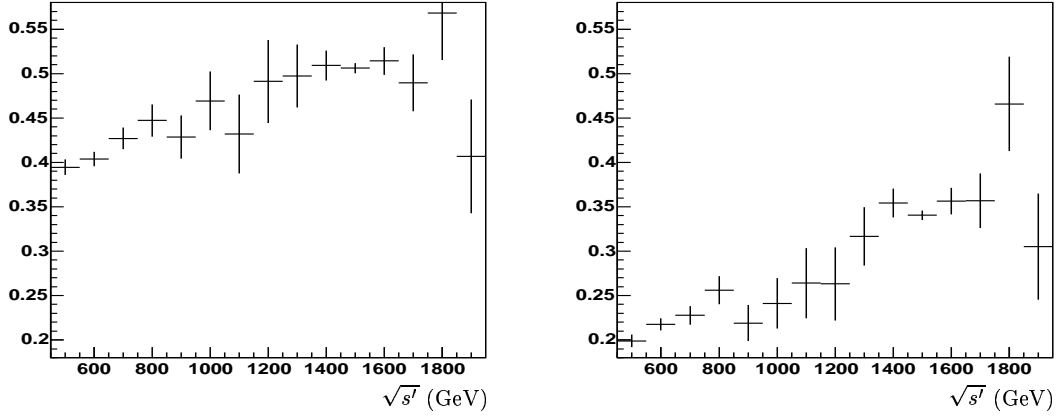


Figure 8: Acceptance as a function of $\sqrt{s'}$ - Z'_{SSM} model - $M = 1.5$ TeV ; left: all events, right: only events with two electrons in the barrel

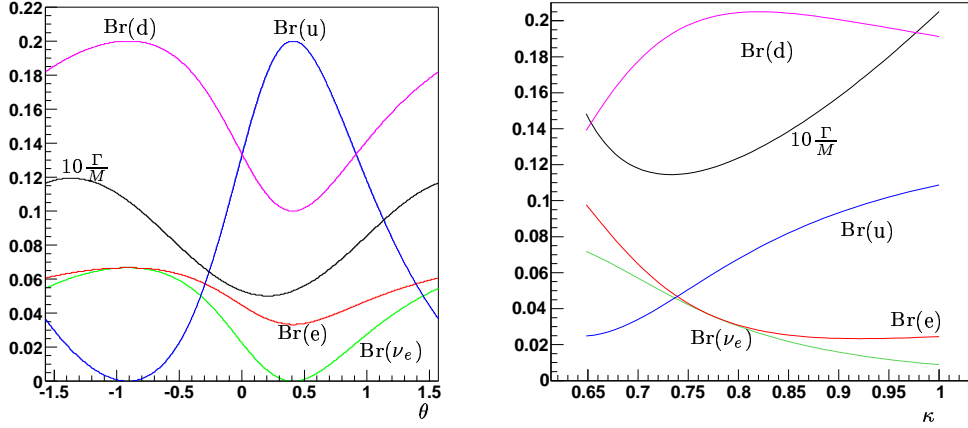


Figure 9: Z' branching ratios and total decay width Γ (over M) as a function of $\sin \theta$ (E_6 , left) and κ (LR , right)

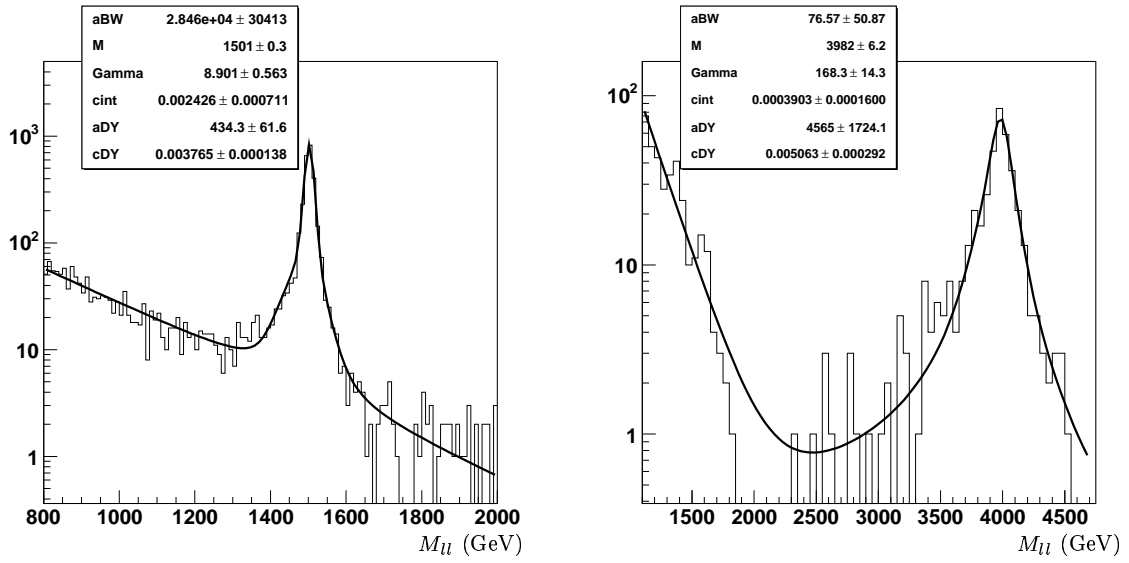
product, therefore it is the $\sigma_{ll} \times \Gamma$ ($= \sigma \times \Gamma_{ll}$) observable instead which is useful in the model discrimination [16].

6.2 Resonance curve fit

The total decay width at generation level is essentially obtained by fitting a relativistic Breit-Wigner function to the invariant mass distribution, with a multiplicative exponential to take into account the deformation of the peak by the interference (and to a lesser extent, the parton luminosity), and an additive exponential to model the Drell-Yan shape:

$$f(M_{ll}) = \frac{a_{BW} M^2 \Gamma^2}{(M_{ll}^2 - M^2)^2 + M^2 \Gamma^2} \times e^{-c_{int} M_{ll}} + a_{DY} e^{-c_{DY} M_{ll}}, \quad (2)$$

where M , Γ , a_{BW} , c_{int} , a_{DY} and c_{DY} are free parameters of the fit.



(a) Z'_η model - $M = 1.5$ TeV

(b) Z'_{KK} model - $M = 4$ TeV

Figure 10: *Fit to the reconstructed invariant mass distribution*

At the reconstruction level, the resonance width is broader, as a consequence of the convolution of the natural decay width and the detector resolution. The latter, independently of the model, was parametrized as explained in the section 5.5 by a sum of two Gaussians - one for the central part and one for the tails. Accordingly, the reconstructed invariant mass distribution is fitted with a function resulting from the convolution (computed numerically) of the former fitting function (equation 2) with the sum of two Gaussians.

The fit is performed in the 0.8 TeV to 2 TeV mass range (1.1 to 4.6 TeV for $M=4$ TeV) for events with two electrons in the barrel. The results of the fit are shown in Fig. 10(a) for one model at $M=1.5$ TeV and in Fig. 10(b) one model at $M=4$ TeV. In table 8, the mass and decay width fitted at the reconstruction level are shown for all studied models; the decay width fitted at the generation level and the calculated prediction are shown as well. A good agreement is obtained for all studied models.

		M_{rec} (GeV)	Γ_{rec} (GeV)	Γ_{gen} (GeV)	$\Gamma_{theo.}$ (GeV)
$M = 1.5$ TeV	SSM	1500.7 ± 0.7	46.6 ± 1.4	47.0 ± 0.9	44.7
	ψ	1500.2 ± 0.3	7.8 ± 0.6	7.1 ± 0.5	8.0
	χ	1500.8 ± 0.4	17.1 ± 0.9	18.4 ± 0.5	17.6
	η	1500.6 ± 0.3	8.9 ± 0.6	9.5 ± 0.4	9.5
	LR	1499.5 ± 0.6	29.7 ± 1.3	32.2 ± 0.8	30.6
$M = 4$ TeV	SSM	$4002. \pm 15.$	$94. \pm 33.$	$97. \pm 19.$	119.
	KK	$3982. \pm 6.$	$168. \pm 14.$	$173. \pm 8.4$	

Table 8: *Results of the fit to the reconstructed dilepton mass for all studied models*

6.3 Leptonic cross section σ_{ll} and $\sigma_{ll} \times \Gamma$

In order to extract the value of the leptonic cross section at the generation level, the number of events in the peak region, practically taken as the $[M-4\Gamma, M+4\Gamma]$ interval, is counted. At the reconstruction level, this range is enlarged by an additional 25 GeV in order to take into account the resolution. The Drell-Yan contribution is not subtracted. The acceptance is corrected using the mean acceptance in this mass range (figure 8). The σ_{ll} at generation and reconstruction levels and the $\sigma_{ll} \times \Gamma$ at reconstruction level results are given in table 9. One can see that the statistical accuracy is high and that this observable is indeed highly discriminant.

It must however be stressed that the final discriminating power will be driven by the control of systematic errors, including:

- uncertainty on the acceptance estimate;
- higher order QCD and QED corrections;
- uncertainty due to the choice of the parton distribution functions;
- bias due to the -very limited- background;
- non perfect Drell-Yan modelisation (as well as its interference with the Z' resonance).

The amplitude of these errors could be reduced by computing a relative cross section, normalizing it by the Z cross section; this would however require a good knowledge of the particle density functions and an accurate control of the energy evolution of the detector performance.

7 Forward-backward asymmetry as a probe of the underlying model

Another signature of the Z' bosons is the forward-backward asymmetry [34, 25] in their production and decays. The differential cross section contains a term proportional to $\cos \theta^*$ (see equation 1), with a form characteristic of spin 1 particles:

$$\frac{d\sigma}{d\cos\theta^*} \propto \frac{3}{8}(1 + \cos^2\theta^*) + A_{FB} \cos\theta^* \quad (3)$$

		$\sigma_{ll}^{gen}(\text{fb})$	$\sigma_{ll}^{rec}(\text{fb})$	$\sigma_{ll}^{rec} \times \Gamma_{rec}(\text{fb} \cdot \text{GeV})$
$M = 1.5 \text{ TeV}$	SSM	78.4 ± 0.8	78.8 ± 1.8	3668 ± 138
	ψ	22.6 ± 0.3	22.7 ± 0.6	178 ± 13
	χ	47.6 ± 0.6	48.4 ± 1.3	828 ± 48
	η	26.2 ± 0.3	25.1 ± 0.6	223 ± 15
	LR	50.8 ± 0.6	51.1 ± 1.3	1515 ± 75
$M = 4 \text{ TeV}$	SSM	0.16 ± 0.02	0.15 ± 0.03	14 ± 6
	KK	2.2 ± 0.07	2.2 ± 0.12	376 ± 37

Table 9: Results on σ_{ll} and $\sigma_{ll} \times \Gamma$ for all studied models

7.1 Angle definitions

High mass dilepton events in pp collisions mainly originate from the annihilation of a - valence or sea - quark with a sea antiquark. As the quark direction is not directly accessible in the data, the angular observables must be carefully chosen in order to extract the asymmetry information.

In all the following, two quantities are considered:

- $\cos\theta^*$ is the angle between the outgoing electron and the quark, in the Z' rest frame, deduced from the generator history.
- $\cos\theta^\otimes$ is the angle between the outgoing electron candidate, in the reconstructed Z' rest frame, and the direction of the reconstructed Z' .

The first quantity will be used to extract the reference asymmetry, whereas the second one will be used as an estimator. The latter is in fact degraded with respect to the $\cos\theta^*$ quantity by three effects:

- the resolution of the electron reconstruction: this was studied in section 5, where the leptons energy and position were found to be correctly reconstructed without any systematic bias⁶. This will therefore only induce a smearing of the estimator.
- the initial state radiation (ISR) of quark/antiquark that modifies the Z' axis with respect to the quark axis. The selection criterion on the angle between leptons in the transverse plane allows to reject events where hard gluons have been emitted. The bias due to this effect should consequently remain limited and will be neglected.
- the quark and the Z' boson being in opposite directions : this especially occurs, when the Z' emerges from the annihilation of a sea quark with a sea anti quark; badly estimating the quark direction leads to a sign flip of the $\cos\theta^\otimes$, and consequently to a (maximally) biased measurement. To control this effect, a study at the generation level is carried out and detailed in the next section.

In Fig. 11, are represented the correlations between $\cos\theta^*$ and $\cos\theta^\otimes$, exhibiting two main behaviours:

- the full correlation, with limited tails due to the leptons characteristics resolution and to the initial state radiation.
- the full anti-correlation, emerging from a bad quark direction estimate.

7.2 Quark and Z' directions at the generation level

In Fig. 12, is shown the distribution of ϵ , defined as the ratio of events for which the scalar product between the quark momentum, in the Z' frame, and the Z' momentum is negative (i.e. the probability to be wrong, when taking the Z' direction as the quark direction); this is plotted as a function of the boson rapidity in several models at $M=1.5$ TeV. This quantity being strongly energy dependent, several cases are considered, depending on the effective Z' mass; the qualitative behaviours are however very similar :

⁶Apart from the case of the end-caps, where the energy calibration is not yet optimal; the Z' boost will therefore be slightly biased but the impact on the results should be minor and will be neglected.

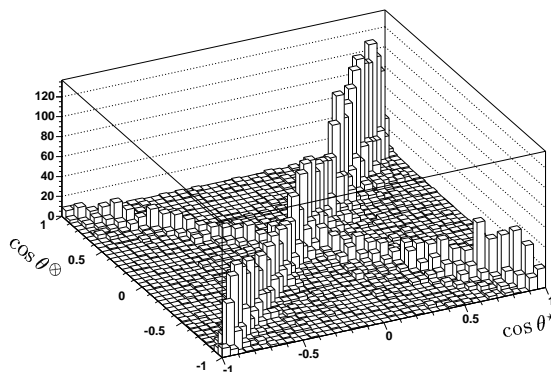


Figure 11: $\cos \theta^*$ vs $\cos \theta^{\otimes}$ - Z'_{SSM} model - $M = 1.5 \text{ TeV}$

- the rapidity increasing, the ratio drops to zero, as it can be expected : the high Z' boost in fact mainly originates from the valence quark.
- at low rapidity, the uncertainty on the quark direction tends to 50%.

These non negligible ambiguities lead to a reduction of the visible asymmetry; this effect, called dilution, will have to be corrected (see details in next section).

The small differences observed between models are due to the differences in u/d parton density functions convoluted with the different coupling constants; the relative differences indeed reflect exactly the differences in flavour of the initial quark/antiquark.

The ϵ quantity is also computed merging the five different event samples generated at $M=1.5 \text{ TeV}$, and fitted by a parabolic function; the result of the fit is superimposed on the same plot. This estimate will be used in all the following, the observed discrepancies between models being treated in the A_{FB} computation as an irreducible source of systematic uncertainty. The latter must be distinguished from the systematic uncertainty associated to the limited statistics of events (reducible by generating more Monte Carlo events).

A similar analysis, of which the results are not presented here, has also been performed for the $M=4 \text{ TeV}$ samples. The above remarks are still valid but, in this case, the ϵ probability drops to zero for lower rapidity : for rapidity greater than 1, taking the Z' direction as the quark is nearly always a valid approximation.

7.3 The dilution impact on the measurement of $A_{FB}(M_U)$

The differential cross section of Z' production being of the form (3), the $A_{FB}(M_U)$ quantity can be deduced by a counting method:

$$A_{FB}(M_U) = \frac{N_+ - N_-}{N_+ + N_-}. \quad (4)$$

where N_+ (N_-) denotes the number of events with the electron in the forward (backward) hemisphere.

At generation level, these quantities are estimated by the following formula:

$$N_+ = \int_0^1 d \cos \theta^* \frac{d\sigma}{d \cos \theta^*}, \quad N_- = \int_{-1}^0 d \cos \theta^* \frac{d\sigma}{d \cos \theta^*}.$$

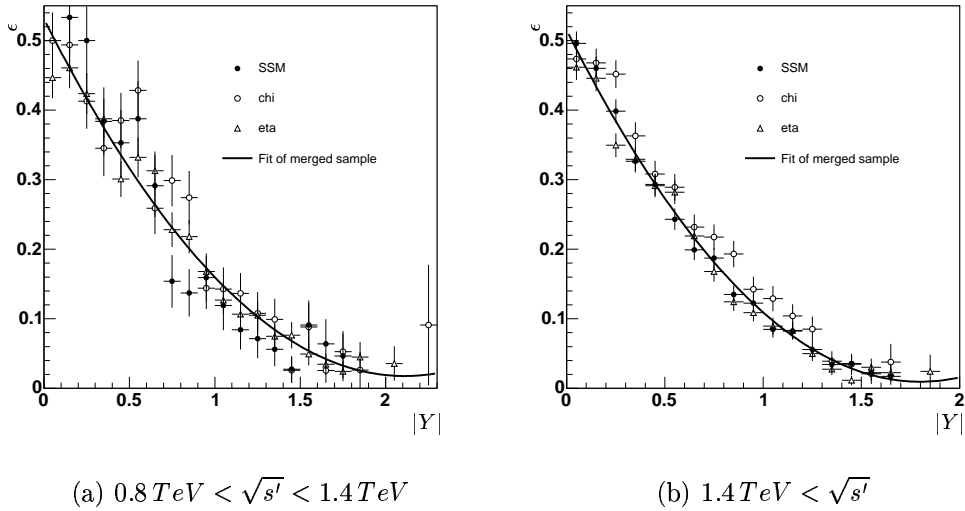


Figure 12: $\epsilon(|Y|)$ at $M=1.5 \text{ TeV}$ in the interference and in the peak regions (to ease the reading, only three models are represented)

The deduced quantity will be used as a reference and called $A_{FB}^{gen}(M_U)$.

A similar definition is taken for the observed asymmetry, $A_{FB}^{obs}(M_U)$, the quantity $\cos \theta^*$ being replaced by $\cos \theta^\otimes$.

Ignoring the detector effects (position/energy resolution) and the transverse momentum of the Z' , a very simple relation between N_\pm^{gen} , N_\pm^{obs} and ϵ , the probability defined in section 7.1, can be written:

$$N_\pm^{obs} = N_\pm^{gen}(1 - \langle \epsilon \rangle) + \langle \epsilon \rangle N_\mp^{gen} \quad (5)$$

And consequently:

$$A_{FB}^{obs} = (1 - 2 \langle \epsilon \rangle) A_{FB}^{gen} \quad (6)$$

As expected, the observed asymmetry is artificially decreased with respect to the one at generation, by the incorrect knowledge of the quark direction; a corrected asymmetry is then defined by:

$$A_{FB}^{cor} = \frac{1}{1 - 2 \langle \epsilon \rangle} A_{FB}^{obs} \quad (7)$$

7.4 Measurement of $A_{FB}(M_U)$

The aforementioned method is very easy to implement and quite efficient but the whole angular information is unfortunately lost, when integrating over an hemisphere; the spin 1 behaviour of the new particle is consequently not tested at all. An alternative natural method could consist in fitting the angular distribution with a function of the form (3); this has however the drawback to strongly depend on the acceptance of the detector. A hybrid method, independent of the detector acceptance, has therefore been developed.

A differential asymmetry is deduced by a classical ‘‘counting method’’, the quantity N_\pm being extracted on a limited $\cos \theta^*$ (or $\cos \theta^\otimes$) range. The running of this new

quantity can be easily deduced from expressions (3) and (4):

$$A_{FB}^{gen}(M_{ll}, \cos \theta^*) = \frac{8}{3} A_{FB}^{gen}(M_{ll}) \times \frac{\cos \theta^*}{1 + \cos^2 \theta^*}$$

$$A_{FB}^{obs}(M_{ll}, \cos \theta^\otimes) = \frac{8}{3} A_{FB}^{obs}(M_{ll}) \times \frac{\cos \theta^\otimes}{1 + \cos^2 \theta^\otimes}$$

Performing an analytical χ^2 fit to this differential asymmetry distributions in the $[0, 1]$ interval then allows to extract the $A_{FB}^{gen}(M_{ll})$ and $A_{FB}^{obs}(M_{ll})$ quantities.

A similar procedure as the one described previously, is applied to correct from the dilution effect and extract $A_{FB}^{cor}(M_{ll}, \cos \theta^\otimes)$. From a technical point of view, the events with a large ambiguity on the quark direction (typically $\epsilon > 0.35$, corresponding to about 25% of the total sample) were found to generate divergences of the fit, when the statistics are low; it was therefore decided to exclude them to compute the quantity A_{FB}^{cor} , the impact of this cut being studied a posteriori.

In order to maximize the discriminating power of the variable, the asymmetry is computed in the vicinity of the resonance in five different mass bins (“on peak” analysis); their widths are taken as the largest value between 40 GeV and 1.2 times the measured natural width. This specific value of 40 GeV has been chosen to limit the impact of the mass experimental resolution (see Fig. 7).

An “off peak” analysis is also performed in $M=1.5$ TeV samples, by extracting the asymmetry in the interference region, requesting the dilepton mass to be between 0.8 TeV and 1.4 TeV; the choice of this interval, not yet optimal for the model discrimination, will be discussed later on.

7.5 The Z'_χ model at $M=1.5$ TeV

The method is first applied to the Z'_χ model⁷ at $M=1.5$ TeV, with a sample size corresponding to an integrated luminosity of $100 fb^{-1}$. The standard selection described in section 5.4 is applied; although the energy calibration of electron/positron is not optimal in the end-caps, the events with leptons in this region have been considered in order to keep reasonable statistics.

In Fig. 13, the fitted distributions of the three differential asymmetries A_{FB}^{gen} , A_{FB}^{obs} , and A_{FB}^{cor} are given for the masses between 1.48 TeV and 1.52 TeV. The good agreement between the data and the fitted functions can be seen as a proof of the spin nature of the intermediate boson. The dilution is also obvious, with a drop of 66% of the observed asymmetry; the dilution is however well corrected, with a good agreement between the asymmetry measured at generation level and the corrected one.

The robustness of the method is checked by varying the upper cut on the ϵ probability; the results are summarized in Fig. 14 and do not exhibit any sizable bias.

The uncertainty in the estimate of the ϵ quantity induces a systematic uncertainty on the A_{FB}^{cor} measurement; an upper limit on it is determined by extracting the ϵ probability from the only χ events sample, that was found to have the most important disagreement with the merged sample and the asymmetries are recomputed. The relative A_{FB}^{cor} fluctuations were found to be of the order of 10%, that is taken as the main source of systematic uncertainty. Some other sources of systematic errors, especially

⁷The Z'_χ model has been chosen for its large asymmetry, which allows to illustrate the method.

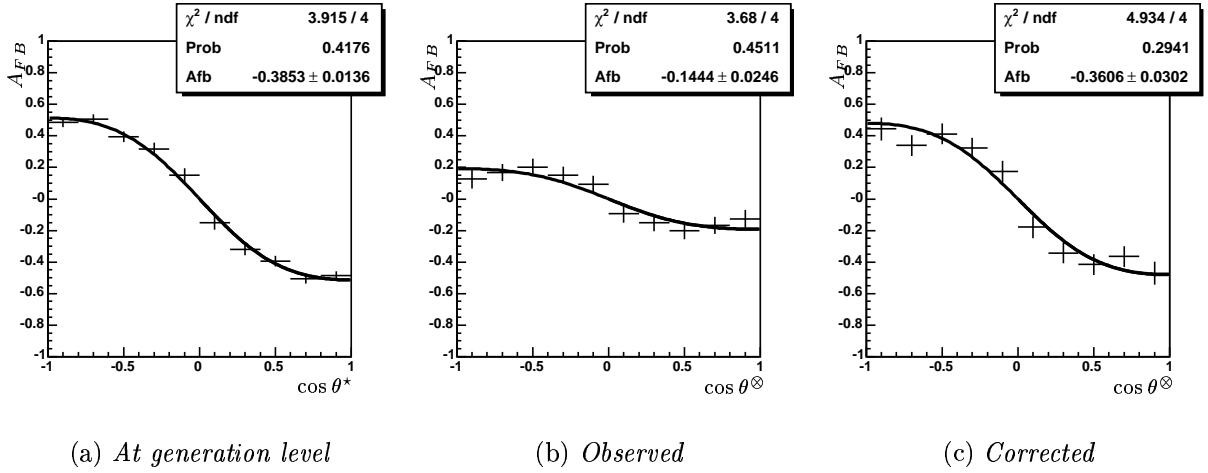


Figure 13: A_{FB} ($1.48 \text{ TeV} < M_{ll} < 1.52 \text{ TeV}$)- Z'_χ model - $M = 1.5 \text{ TeV}$

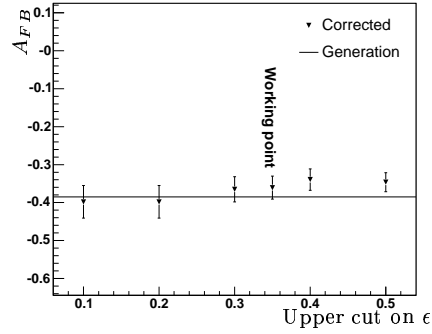


Figure 14: $A_{FB}(M_{ll})$ (stat.errors only) as a function of ϵ upper cut - Z'_χ model - $M = 1.5 \text{ TeV}$

the impact of the choice of the particle density functions, will have to be studied in a refined analysis.

The complete output of the on peak analysis is summarized in Fig. 15, with the five different asymmetries extracted around the Z' resonance. With reduced statistics, the errors are larger but the general remarks are still valid: due to the dilution effect, the observed asymmetry is reduced with respect to the one computed at generation level; applying a correction deduced from the ϵ distribution is an efficient way to recover from this effect.

Finally, the result of the off peak analysis is given in table 10. The method remains efficient, with however an enhanced systematic error due to the uncertainty on the ϵ determination over a wide mass range.

7.6 The on peak analysis

The A_{FB} measured at generation level are plotted for all the models studied in Fig. 16. The notable differences show the high discriminating power of the asymmetry.

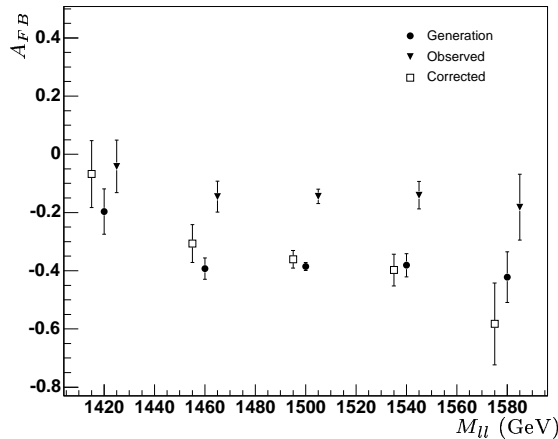


Figure 15: *Summary of the on peak analysis : $A_{FB}(M_{ll})$ (stat.errors only) - Z'_χ model - $M = 1.5 TeV$*

	Generation level	Observed	Corrected
A_{FB}	-0.439 ± 0.019	-0.179 ± 0.032	-0.353 ± 0.039

Table 10: *Off peak A_{FB} (stat. errors only) - Z'_χ model - $M = 1.5 TeV$*

On table 11, are summarized the observed and corrected asymmetries (with the generation one) in the central bin of dilepton mass (i.e. containing the highest statistics); as already pointed in the previous section, the implemented correction is an efficient way to recover from the incomplete knowledge of the quark direction. It is worth noting that without this correction, the discrimination between models would be much more difficult.

The systematic uncertainty associated to the ϵ parametrization was evaluated for each model in the same way as in previous section and is confirmed to be of the order of 10%. It is assumed to be the largest source of systematic uncertainty as compared to the ones due to higher order QCD and QED corrections and to the choice of the parton distribution functions.

Finally, the performance of the procedure is summarized for all mass bins and all models in Fig. 17 (i.e. 25 independent analyzes). In Fig. 17(a) are represented the deviations of observed values with respect to the value computed at generation level; it is doubly peaked around ± 1.5 , the samples with a positive (negative) asymmetry populating the positive (negative) regions. This results once again from the dilution effect; this systematic bias is even more striking in Fig. 17(b), showing the distribution of the absolute value of the same quantity (these deviations depending strongly on the asymmetry values, these studies must not be considered as a quantitative estimate of the dilution effect; they have been performed only to be a reference measurement in the performance study of the correction procedure detailed thereafter).

The efficiency of the correction procedure is illustrated in Fig. 17(c): the bias and the tail vanish; with limited statistics, the measurement exhibits a gaussian behaviour centered around 0 with a width slightly greater than 1 (showing the need to carefully

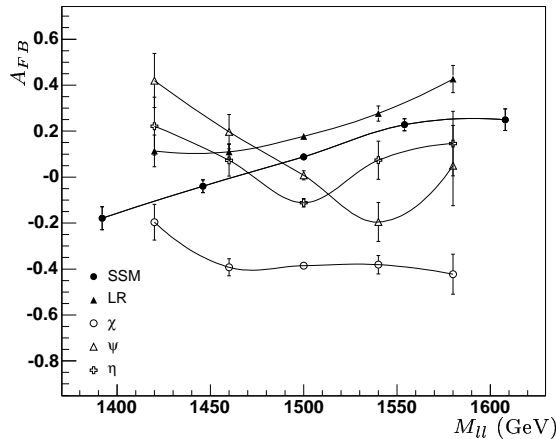


Figure 16: *On peak analysis : results at generation level*

Model	$\int \mathcal{L}(fb^{-1})$	Generation	Observed	Corrected
1.5 TeV				
<i>SSM</i>	100	$+0.088 \pm 0.013$	$+0.060 \pm 0.022$	$+0.108 \pm 0.027$
χ	100	-0.386 ± 0.013	-0.144 ± 0.025	-0.361 ± 0.030
η	100	-0.112 ± 0.019	-0.067 ± 0.032	-0.204 ± 0.039
η	300	-0.090 ± 0.011	-0.050 ± 0.018	-0.120 ± 0.022
ψ	100	$+0.008 \pm 0.020$	-0.056 ± 0.033	-0.079 ± 0.042
ψ	300	$+0.010 \pm 0.011$	-0.019 ± 0.019	-0.011 ± 0.024
<i>LR</i>	100	$+0.177 \pm 0.016$	$+0.100 \pm 0.026$	$+0.186 \pm 0.032$
4 TeV				
<i>SSM</i>	500	$+0.138 \pm 0.099$	$+0.006 \pm 0.183$	$+0.265 \pm 0.260$
<i>KK</i>	500	$+0.491 \pm 0.028$	$+0.189 \pm 0.057$	$+0.457 \pm 0.073$

Table 11: *Measured on peak A_{FB} for all studied models in the central mass bin.*

study the various sources of systematic uncertainty).

7.7 The off peak analysis

The off peak ($0.8 \text{ TeV} < M_U < 1.4 \text{ TeV}$) asymmetry extraction, summarized in table 12, provides a measurement complementary to the on peak one. Considering only the statistical errors, the agreement between the corrected asymmetry and the one computed at generator level is found to be slightly worse than in the on peak analysis. This can be explained by the inability to correctly estimate the ϵ probability over a wide mass range, leading to an enhanced associated systematic error.

In a refined analysis, it would be possible to take full benefit of the off peak informations, by performing independent analyzes on narrower mass bins, where the ϵ quantity can be accurately estimated (providing the availability of a large quantity of Monte Carlo events). It is worth noting that even with a limited statistic, such analysis would provide meaningful informations : this can be seen in Fig. 18, where are represented

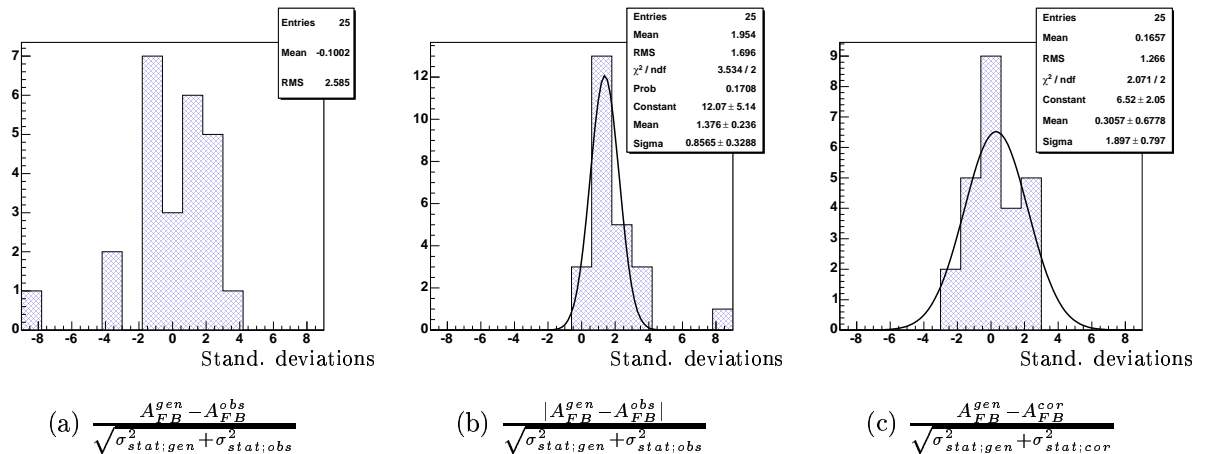


Figure 17: *Performance summary for the complete on peak analyzes of the five models at $M=1.5$ TeV.*

the asymmetries computed in five narrow bins of 8 times the measured width around the Z' resonance. The latter are computed at generation level (i.e. not involving the ϵ probability) for a luminosity of $100 fb^{-1}$, showing the discrimination potential of such measurements.

Model	$\int \mathcal{L}(fb^{-1})$	Generation	Observed	Corrected
1.5 TeV				
SSM	100	$+0.077 \pm 0.025$	$+0.086 \pm 0.038$	$+0.171 \pm 0.045$
χ	100	$+0.440 \pm 0.019$	$+0.180 \pm 0.032$	$+0.354 \pm 0.039$
η	100	$+0.593 \pm 0.016$	$+0.257 \pm 0.033$	$+0.561 \pm 0.039$
ψ	100	$+0.673 \pm 0.012$	$+0.294 \pm 0.033$	$+0.568 \pm 0.039$
LR	100	$+0.303 \pm 0.022$	$+0.189 \pm 0.033$	$+0.327 \pm 0.040$

Table 12: *Measured off peak A_{FB} for all studied models at $M=1.5$ TeV*

8 Conclusions

The potential of the Atlas detector to measure the total decay width and the leptonic forward backward asymmetry in several Z' models has been studied. These two variables were found to be correctly measured with a realistic luminosity and to bring informations on the underlying model. Additional observables may be needed to consolidate the discrimination; some have been already proposed in other articles and consist in:

- The Z' rapidity distribution [16]. This would especially allow to extract the couplings constant to quarks involved in the initial state.

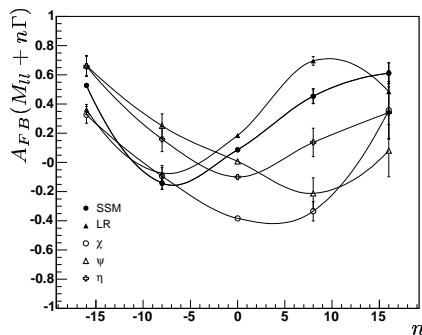


Figure 18: *Prospective off peak analysis (at generation level) - $M=1.5$ TeV*

- The ratio of cross sections in different rapidity bins [43]:

$$r_{Y1} = \frac{\int_{-Y1}^{Y1} \frac{d\sigma}{dY} dY}{\left[\int_{-Y_{max}}^{-Y1} + \int_{Y1}^{Y_{max}} \right] \frac{d\sigma}{dY} dY}, \quad \text{with } 0 < Y1 < Y_{max}.$$

- The forward-backward asymmetry as a function of the Z' rapidity [1, 44, 45] is another way to probe the quark couplings constant.

Then, a global procedure will have to be defined to combine all these results (as well as the one of potential analysis with different decay channels: $\tau^+\tau^-$, jet-jet or four-fermions). This could consist in a global fit or in the extraction of the four “normalized couplings” proposed in the reference [46].

Acknowledgments

The authors specially thank **Georges Azuelos** and **Samir Ferrag**, the coordinators of the ATLAS exotics group, for helpful discussions and critical suggestions. Thanks also go to **Giacomo Polesello**, the ATLAS physics coordinator. We also owe much gratitude to **Armin Nairz** and **Nectarios Benekos** for their help and support for the full simulation. Thanks also go to **Stathes Paganis** for his help on the calibration.

References

- [1] P.Langacker, R.W.Robinett, J.L.Rosner, Phys. Rev. D30 (1984) 1470.
- [2] F.del Aguila, M.Quiros, F.Zwirner, Nucl. Phys. B287 (1987) 419.
- [3] V.Barger, N.G.Deshpande, J.L.Rosner, K.Whisnant, Phys. Rev. D35 (1987) 2893.
- [4] L.Hewett, T.G.Rizzo, Phys. Rep. 183 (1989) 193.
- [5] F.del Aguila, Acta Phys. Polon. B25 (1994) 1317, hep-ph/9404323.
- [6] M.Cvetič, S.Godfrey, “Discovery and identification of extra gauge bosons”, Barklow, T.L. (ed.) et al.: *Electroweak symmetry breaking and new physics at the TeV scale* 383-415, hep-ph/9504216.

- [7] M.Cvetič, P.Langacker and B.Kayser, Phys. Rev. Lett. 68 (1992) 2871.
- [8] V.Barger, T.G.Rizzo, Phys. Rev. D41 (1990) 946.
- [9] R. Foot, O.F. Hernández and T.G. Rizzo, Phys. Lett. B246 (1990) 183.
- [10] T.K. Kuo and N. Nakagawa, Phys. Rev. Lett. 57 (1986) 1669.
- [11] R.Casalbuoni et al., Eur.Phys. J C18 (2000) 65.
- [12] T.Han et al., Phys. Rev. D67 (2003) 095004.
- [13] J.L.Hewett, B.Lillie, T.G.Rizzo, JHEP 0410 (2004) 014.
- [14] T.G. Rizzo, Phys. Rev. D61, 055005 (2000) and Phys. Rev. D64, 015003 (2001).
- [15] B.C. Allanach et al., JHEP 0009 (2000) 019;
 B.C. Allanach et al., “Exploring Small Extra Dimensions at the Large Hadron Collider”, ATL-PHYS-2002-031 (2002);
 C.Collard et al., “Prospects for Study of Randall-Sundrum Gravitons in the CMS Experiment”, CMS-NOTE-2002-050 (2002).
- [16] M.Dittmar, A.Nicollerat, A.Djouadi, Phys. Lett. B583 (2004) 111.
- [17] K.Hagiwara et al. (Particle Data Group), Phys. Rev. D66 (2002) 010001.
- [18] G.Azuelos, G.Polesello, “Prospects of the detection of Kaluza-Klein excitations of gauge bosons in the ATLAS detector at the LHC”, SN-ATLAS-2003-023 (2003).
- [19] M.Cvetič, P.Langacker, Phys. Rev. D46 (1992) R14.
- [20] V.Barger, K.Whisnant, Phys. Rev. D36 (1987) 3429.
- [21] A. Ferrari et al., Phys. Rev. D62 (2000) 013001.
- [22] J.Shank et al., “Studies of A^0 , Z' and W' Production and Detection with The ATLAS Muon Detector”, ATLAS Internal Note MUON-NO-161 (1997).
- [23] J.D.Anderson, M.H.Austern, R.N.Cahn, Phys. Rev. D46 (1992) 290.
- [24] M.H.Austern, “ Z' Phenomenology”, Ph.D. Thesis (1994), Lawrence Berkeley Laboratory, University of California.
- [25] The LEP Collaborations ALEPH, DELPHI, L3, OPAL, the LEP Electroweak Working Group, the SLD Electroweak and Heavy Flavour Groups, “A Combination of Preliminary Electroweak Measurements and Constraints on the Standard Model”, CERN-EP/2003-091, hep-ex/0312023.
- [26] M.Carena et al., Phys. Rev. D70 (2004) 093009.
- [27] J.L.Rosner, Phys. Lett. B387 (1996) 113.
- [28] F. Abe et al. (CDF coll.), Phys. Rev. Lett. 79 (1997) 2192;
- [29] T.G.Rizzo, Phys. Rev. D61 (2000) 016007.
- [30] T.G.Rizzo, “Phenomenology of higgsless electroweak symmetry breaking”, SLAC-PUB-10431, hep-ph/0405094.
- [31] ATLAS Detector and Physics Performance Technical Design Report, Volume II, CERN/LHCC/99-15 (1999).
- [32] PYTHIA, T.Sjöstrand et al., Comp.Phys. Comm. 135 (2001) 238.
- [33] ATHENA, <http://www.wlap.org/atlas/computing/tutorials/athena/2002/>

- [34] M.Böhm, W.Hollik, Forward-Backward Asymmetries, CERN yellow report 89-08 (09/1989).
- [35] M.Dittmar, Phys. Rev. D55 (1997) 161.
- [36] T.G.Rizzo, JHEP 0306 (2003) 021.
- [37] ATLAS DC1 Project Report (2001).
- [38] R.Brun, F.Carminati, “GEANT Detector Description and Simulation Tool”, W5013, CERN Programm Library, CERN, Geneva, Switzerland; “A Simulation Toolkit”, Nucl. Instr. and Meth. A506 (2003) 250.
- [39] http://atlas.web.cern.ch/Atlas/GROUPS/LIQARGSOFF/Electron_Photon/eid.html
- [40] B.Mellado, S.Paganis, W.Quayle, Sau Lan Wu, “ATLAS Electromagnetic Calorimeter calibration and shower isolation studies with an application to the $H \rightarrow ZZ^{(*)} \rightarrow 4e$ analysis”, ATLAS internal note, ATL-PHYS-2004-005 (2004).
- [41] M.Dittmar et al., Phys. Rev. D56 (1997) 7284.
- [42] U. Baur et al., Phys. Rev. D65 (2002) 033007.
- [43] F.del Aguila, M.Cvetič, P.Langacker, Phys. Rev. D48 (1993) R969.
- [44] J.L.Rosner, Phys. Rev. D35 (1987) 2244.
- [45] M.Schäfer, “Study of $Z' \rightarrow e^+e^-$ in full simulation with regard to discrimination between models beyond the Standard Model with ATLAS”, Diploma Thesis, Grenoble (September 2004), LPSC-04-59.
- [46] F.del Aguila, M.Cvetič, P.Langacker, Phys. Rev. D52 (1995) 37.
- [47] M.C.Cousinou, “Search for a W' in the $l\nu$ channel”, ATL-Phys-94-059 (1994).